Appl. Phys. B 90, 561–567 (2008)
DOI: 10.1007/s00340-007-2893-2

Applied Physics B
Lasers and Optics

A. WELLER
F.C. LIU
R. DAHINT
M. HIMMELHAUS✉,*

Whispering gallery mode biosensors in the low-Q limit

Angewandte Physikalische Chemie, Universität Heidelberg, INF 253, 69120 Heidelberg, Germany

Received: 7 July 2007/Revised version: 2 November 2007
Published online: 12 February 2008 • © Springer-Verlag 2008

ABSTRACT Whispering gallery modes (WGM) of dye-doped polystyrene beads with diameters from 20 down to 1.5 μm are studied with respect to their appearance and linewidth by excitation of the entire mode spectrum within the emission range of the dye. The lowest order ($q = 1$) modes, which travel most closely to the inner particle surface, are assigned to their individual quantum numbers by means of a least-square-fit, resulting in a precise determination of particle radius and eccentricity. On this basis, the suitability of these microscopic cavities for applications in optical (bio-)sensing is explored. Due to the low quality (Q) factors of these small cavities, particles with diameters below 6 μm exhibit only $q = 1$ modes, thereby causing a drastic simplification of the WGM spectrum. In such spectra, the shift in the WGM positions upon molecular adsorption can be easily monitored, as we demonstrate for the adsorption of bovine serum albumin as well as multiple layers of polyelectrolytes onto the surface of particles with 2 μm diameter. Mie simulations are used to confirm our findings. With a mass sensitivity limit of 3 fg, these microscopic sensors are highly competitive in the field of label-free detection techniques. Moreover, their small size and the simplified, dye-mediated excitation and detection scheme may pave the way to remote in-vitro biosensing in the future.

PACS 07.07.Df; 42.60.Da; 42.70.Jk

1 Introduction

Optical microcavities confining light to mesoscopic volumes have recently become attractive tools in various fields of basic and applied research [1–3], ranging from fundamental studies on quantum electrodynamics, such as Purcell enhancement [4] and emitter-photon coupling [5, 6], to more practical fields, like the development of microscopic laser sources [7, 8], optical filters [9], and transducer mechanisms for optical sensing [10–12]. For (bio-)sensing, only low-loss cavities have been recognized so far, due to their high resolving power and correspondingly high sensitivity to changes in their immediate environment. However, this concept is hampered by limited miniaturization potential and demands on mechanical precision. Here, we explore the potential of dye-doped polymer beads of 2 μm diameter for biosensing in the high loss regime. The key to this is the $1/R$ dependence in the modes' wavelength shift on the particle radius, R, due to molecular adsorption, which may overcompensate limitations associated with their increased linewidths [13]. The $1/R$ law will be proven experimentally by polyelectrolyte adsorption and numerically by Mie calculations, thereby confirming an unrivaled sensitivity limit for label-free biosensing of 3 fg of analyte.

Dielectric microcavities fabricated from low loss media with sizes from several tens to hundreds of microns have been renowned for the highest Q-factors ever achieved in optical resonators with values close to 10^{10} [14]. The extreme narrow linewidths $\Delta\lambda_\nu$ of the cavity modes, which are connected with the Q-factor Q_ν and the peak position λ_ν of mode ν according to $Q_\nu = \lambda_\nu/\Delta\lambda_\nu$, suggest an extraordinary resolving power $\Re = \lambda/\delta\lambda_{\min}$, where $\delta\lambda_{\min} \sim \Delta\lambda_\nu$ is the least resolvable wavelength difference of the system. The high-Q modes in such systems are so-called whispering gallery modes (WGM), which can be viewed as light traveling along the inner circumference of the particles at incidence angles above the critical angle for total internal reflection (TIR) (cf. Fig. 1a). On the outside, an exponentially decaying evanescent field exists, which is sensitive to changes of the dielectric function in the intimate vicinity of the cavity, thus facilitating the fabrication of highly sensitive microscopic biosensors, where either the shift in the resonance position [12] or the change of the Q-factor [11] due to biomolecular adsorption on the outer cavity surface can be detected with a mass sensitivity of up to 6 pg/mm^2 [15]. This concept of high-Q WGM sensing is hampered however, by several obstacles, particularly with respect to biotechnological demands for miniaturization, multiplexing, and simplicity of use. The deeper cause for such discords is the limitation in minimum particle size of WGM cavities imposed by the demand for high Q-factors.

Losses in dielectric WGM cavities originate from material absorption and scattering, scattering at the interface due to surface roughness, and a loss related to the curvature of the reflecting surface. The latter becomes increasingly important with decreasing R due to the increasing average incidence angle of the circulating light, which finally leads to a violation

✉ Fax: +81-426-45-4758,
E-mail: michael.himmelhaus@urz.uni-heidelberg.de
*_Present address_: Fujirebio, Inc., Hachioji 192-031, Japan
The online version of this article (doi:10.1007/s00340-007-2893-2) contains supplementary material, which is available to authorized users.

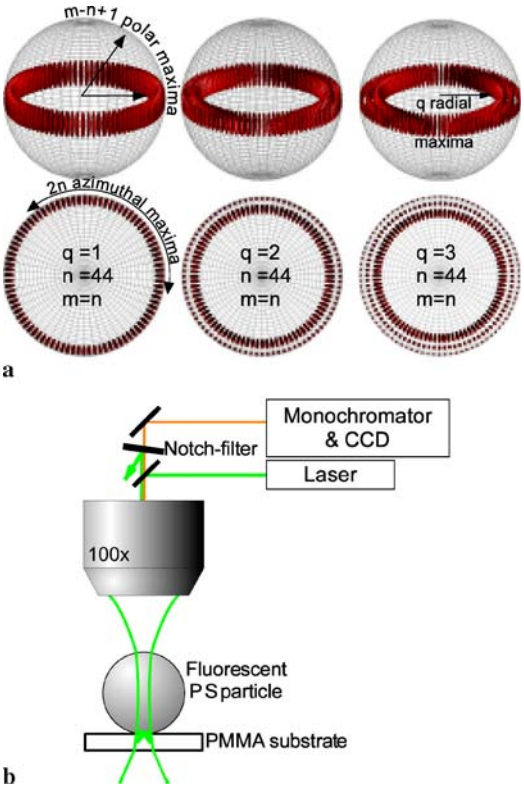

FIGURE 1 (**a**) The plots exemplify the field intensity distribution for $n = m = 44$ modes with $q = 1$, 2, and 3, respectively. (**b**) Scheme of the experimental set-up for excitation and detection of WGM in fluorescent PS beads by means of a Raman microscope

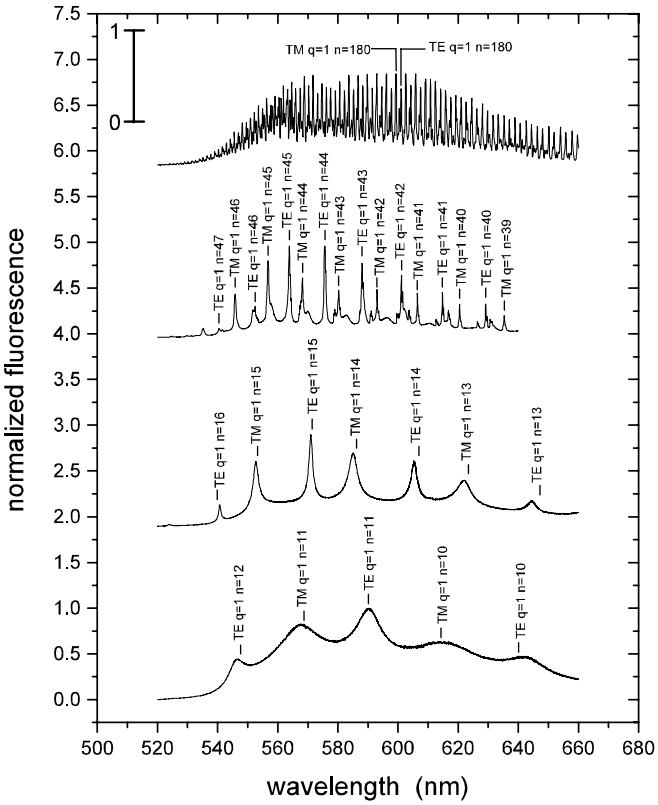

FIGURE 2 Fluorescence emission from polystyrene (PS) particles containing a fluorescent dye for different particle sizes. The emission spectra are strongly modulated by whispering gallery mode (WGM) excitations. The mode assignments result from the fitting of the particle radii as described in the methods' section. Particle diameters (from top): 20, 6, 2, 1.5 μm

of the TIR condition below a value $R_{\min}$. A simple geometric consideration that replaces the path of the WGM inside of the cavity by a polygon of side-length λ yields

$$R_{\min} = \frac{\lambda}{n_c} \frac{1}{\pi - \theta_{\text{crit}}},$$

where θ_{crit} (in rad) is the critical angle, n_c the refractive index of the cavity, and λ the vacuum wavelength of the circulating light. $\lambda = 500$ nm and $n_c = 1.5$, predicts $R_{\min} = 200$ nm for a cavity in air. Below this size, the cavity has lost all capability to trap photons by TIR. In practice, however, the other loss mechanisms add to this basic limit. The smallest dielectric particles, for which WGM excitation has been reported to date, are polystyrene (PS) spheres with a diameter of 2 μm [16]. The observed low Q-factors reduce the resolving power of the system, so that particles in this size regime have not been considered for (bio-)sensing applications so far. To achieve Q-factors sufficiently high for sensing, particles should be made from materials with low internal scattering, such as silica, and should have diameters of some hundreds of microns. This size limitation, however, harshly restricts the implementation of WGM biosensors. As shown in Fig. 2 for a 20 μm sphere, the WGM spectrum of particles with diameters exceeding ten microns is very complex, thus complicating tracing of any changes. Therefore, in practice, a single mode is selected as sensing mode by coupling light of sufficiently narrow bandwidth into the cavity from the outside. Efficient coupling requires the spatial overlap of the evanescent fields of the cavity and the source of excitation, e.g., the core of an optical fiber, a fiber coupler, or the waist of a sharply focused Gaussian laser beam [2]. The distance between the evanescent fields of excitation source and particle, respectively, must be controlled with nanometer precision, thereby complicating the applicability of the system.

We have, therefore, investigated the potential of small particles with low Q-factors for (bio-)sensing applications. Our study is based on an important finding. As has been shown by Schweiger and Horn [17], the mode spacing in spherical cavities depends on size and refractive index of the cavity, and – typically to a lesser extent – on the refractive index of the environment. In the case of adsorption of a thin layer of thickness d and excess polarizability α_{ex} on the outer cavity surface, this translates into a size-dependent wavelength shift Δλ. Arnold and coworkers [13] derived the sensitivity, $\Delta\lambda/\lambda$, of WGM biosensors for the adsorption of very thin adsorption layers ($d \ll \lambda$) from a perturbation theoretical approach.

They showed that $\Delta\lambda/\lambda \sim \alpha_{\text{ex}}/R$, and confirmed this finding experimentally for particles with high Q-factors, i.e. for particles with diameters of some tens to some hundreds of microns. As we will show below, this power law remains valid also in the low-Q regime for cavities as small as 2 μm in diameter. Therefore, the loss in resolving power may be overcompensated by an increase in sensitivity, i.e. a larger resonance shift, when reducing the size of the particle. In addition, its total surface area decreases with $1/R^2$, so that for fixed resolving power the detection limit scales with $1/R^3$, i.e. less and less biomolecules may be detected with increasing sensitivity.

As we will also demonstrate, one further advantage of using small particles is their simple mode spectrum, which can be entirely excited and used for sensing without causing any ambiguity. Thus, the crucial evanescent field coupling can be avoided, e.g. by exciting the mode spectrum from the inside of the cavity by means of a fluorescent dye, thus largely widening applicability and ease of usage of WGM sensors and making them potential candidates for in-situ micro-sensing applications.

2 Experimental

2.1 *Chemicals*

Sulfonated polystyrene (PS) particles of different sizes (Polysciences), xylene (96%, Merck), nile red fluorescent dye (HPLC grade, Fluka), poly(allylamine hydrochloride) (PAH, MW 15 000 Da) and poly(sodium 4-styrenesulfonate) (PSS, MW 70 000 Da), and bovine serum albumin (BSA, 98%, MW 66 kDa) (all Sigma Aldrich) were used as received. Deionized water ($> 18\,\mathrm{M\Omega\,cm}$) was produced by a MilliQ plus system.

2.2 *Inking*

A 500 µl saturated solution of nile red in xylene was placed on top of 8 ml of a PS particle suspension diluted ~ 40 fold by means of deionized water. The resulting phase-separated system was gently shaken until the xylene had evaporated. The remaining aqueous phase was centrifuged at 5000 rpm and the supernatant removed in order to obtain a concentrated suspension of dye-inked PS particles.

2.3 *Coating*

2.3.1 Bovine serum albumin. 1 mg of BSA was dissolved in 1 ml of deionized water. For coating of the PS beads with BSA, the particles were first rinsed with pure water three times (using a microliter syringe) and then dried in air for 15 min. Subsequently, 20 µl of the BSA solution were placed on the particles for 30 min. After removal of the BSA solution, the particles were again rinsed three times with pure water and then dried in air. The emission spectra before and after BSA adsorption were acquired after the respective drying processes.

2.3.2 Polyelectrolytes. PAH and PSS were both adsorbed from either salt-free or 0.5 M NaCl aqueous solutions at a concentration of 1 mg/ml, respectively. We used the same procedure for coating with polyelectrolytes (PE) as that described above for BSA adsorption, i.e. three washing steps were applied before and after exposure of the particles to the particular PE solution, respectively.

2.4 *WGM measurements*

For the study of dye-inked PS beads with diameters from 1.5 to 20 µm, a Dilor LabRam Raman microscope was used to excite the dye and detect the radiation scattered from the particles as illustrated in Fig. 1b. The particles were first immobilized on a poly(methylmethacrylate) (PMMA) substrate and then placed in the focus of a 100× objective. For excitation of the fluorescent dye, a cw Ar ion laser was coupled into the microscope at a radiant power of 15 mW, yielding a focus of 3 µm diameter. The emitted light was re-collected by the 100× objective and separated from the excitation by means of a Notch filter. The spectral range of the detection unit was 520–660 nm at an optical resolution of $\delta\lambda = 0.03$ nm.

2.5 *Determination of particle radii*

WGM are easiest described in terms of spherical coordinates r, θ, and φ, where r is the radial coordinate, θ the polar angle, and φ the azimuthal angle. The boundary conditions $r < R, 0 < \theta < \pi$, and $\varphi = 2\pi n + \varphi$, where n is an integer, lead to a quantization by means of three quantum numbers q, n, and m. Thereby, q is equivalent to the number of intensity maxima in radial direction, $2n$ corresponds to the number of intensity maxima in azimuthal direction (for $n = m$), i.e. along the sphere's circumference, and $m - n + 1$ gives the number of intensity maxima in polar direction. Figure 1a visualizes the intensity distribution for $n = m = 44$ modes with $q = 1, 2$, and 3, respectively. Obviously, $q = 1$ modes have a field distribution closest to the particle surface. Therefore, they exhibit the highest Q-factors.

For accurate determination of the sensitivity of a spherical WGM sensor, the precise knowledge of the particle radius R is of utmost importance as the wavelength shift due to changes in the immediate environment of the particle is inversely proportional to R (cf. (4)). To extract this value from the WGM spectra with high precision, we proceed as follows. As pointed out by Oraevsky [18], the resonance frequencies of the $q = 1$ modes can be approximated by the following analytical expressions for transverse electric (TE) and transverse magnetic (TM) fields, respectively:

$$\omega_n^{\mathrm{TE}} \approx \frac{c}{R\sqrt{\varepsilon\mu}}\left[\nu + 1.85576\nu^{\frac{1}{3}} - \frac{1}{\mu}\sqrt{\frac{\varepsilon\mu}{\varepsilon\mu - 1}}\right], \tag{1a}$$

$$\omega_n^{\mathrm{TM}} \approx \frac{c}{R\sqrt{\varepsilon\mu}}\left[\nu + 1.85576\nu^{\frac{1}{3}} - \frac{1}{\varepsilon}\sqrt{\frac{\varepsilon\mu}{\varepsilon\mu - 1}}\right]. \tag{1b}$$

Here, $\nu = n + 0.5$, where n is the WGM quantum number of the azimuthal angle φ, and ε and μ are the dielectric permittivity and magnetic permeability, respectively, of the particle. For polymer beads holds $\mu = 1$, while ε can be calculated via the Maxwell relation $\varepsilon = n_c^2$. The quantum number m of the polar angle θ does not enter these formulas due to the spherical symmetry of the system. For deviations from spherical symmetry, the degeneration in m is resolved. For small deviations, the mode splitting can be written [18]

$$\omega_{mn} \approx \omega_n\left[1 - \frac{\mathrm{d}R}{R}\left(2 + 3\frac{n^2 - m^2}{n^2}\right)\right], \tag{2}$$

where $\mathrm{d}R$ is the deviation of the minor axis of the spheroid from the initial radius of the sphere.

For evaluation of the measured WGM spectra, we combined (1) and (2) by defining the parameter

$$P = \left[\frac{1}{R} - 2\frac{\mathrm{d}R}{R^2}\right]^{-1}.$$

Then, the WGM resonance positions can be written as

$$\lambda_n^{\mathrm{TE}} \approx P * \left(\frac{1}{2\pi\sqrt{\varepsilon\mu}} \left[\nu + 1.85576\nu^{\frac{1}{3}} - \frac{1}{\mu}\sqrt{\frac{\varepsilon\mu}{\varepsilon\mu - 1}} \right] \right)^{-1}, \tag{3a}$$

$$\lambda_n^{\mathrm{TM}} \approx P * \left(\frac{1}{2\pi\sqrt{\varepsilon\mu}} \left[\nu + 1.85576\nu^{\frac{1}{3}} - \frac{1}{\varepsilon}\sqrt{\frac{\varepsilon\mu}{\varepsilon\mu - 1}} \right] \right)^{-1}. \tag{3b}$$

Equation (3) can be used for precise determination of the particle radius and eccentricity by a least-square fit to the experimentally determined WGM positions as a function of the parameter P. Since the WGM quantum number n is also unknown, the least-square fit is repeatedly performed for a whole range of n, which has been estimated roughly from the nominal particle size before starting the fitting. For example, for the 2 μm beads, n was varied from 1 to 100. Then, that value of n is selected, for which the χ^2 deviation of the fit is minimal, thereby also obtaining the best fit-value for the parameter P. From the latter, the particle radius and its deviation $\mathrm{d}R$ can be calculated.

2.6 *Simulations*

Mie-calculations were performed with mathematica 3.0 for windows (Wolfram Research) on a personal computer. For calculation of the WGM resonance shifts due to coating of the particles with an adsorbate, we used the theory of Aden and Kerker [19] for a homogeneously coated sphere, however, in the formulation of Quirantes and Delgado [20] due to the better suited representation of the Mie coefficients. The refractive indices were $n_{\mathrm{c}} = 1.59$ for the PS particle, $n_{\mathrm{PE}} = 1.47$ for the PE coatings [21], and $n_{\mathrm{env}} = 1.0$ for the environment of the coated particle. The step size was set to $\mathrm{d}\lambda = 0.05$ nm to achieve sufficient wavelength resolution [22]. During the simulations, which were performed for the smallest particle size of 2 μm diameter only, we did not find any significant contributions from Mie coefficients, a_n, b_n, with $n > 20$. Therefore, the sum over n for calculating the scattering cross sections was limited to $n_{\max} = 30$. Selected calculations performed with $n_{\max} = 100$ did not show any differences in the results. This observation is in excellent agreement with a study by Roll et al. [22], who found that the contribution of Mie coefficients above the expansion order $n_{\mathrm{trunc}} = 2\pi n_{\mathrm{c}} R/\lambda$ is negligible, which yields $n_{\mathrm{trunc}} = 17$ for a WGM positioned at $\lambda = 600$ nm and the 2 μm particles studied here.

3 Results and discussion

Excitation of the dye molecules inside of the particles by means of the Raman microscope is highly effective as its tight laser focus can be placed into the center of the beads, thereby yielding perpendicular incidence across the entire illuminated area on the bead surface and thus minimizing reflection losses as well as lensing effects. The excited dye molecules emit in arbitrary direction, in this manner accidentally also populating cavity modes. Accordingly, particularly dye molecules in proximity of the particle surface contribute to WGM excitation. While light in other directions is immediately scattered to the outside, the modes gain steadily in intensity and may also experience further increase due to stimulated emission. Therefore, as shown in Fig. 2 for different particle sizes, the fluorescence spectra are strongly modulated by the cavity modes, which can be assigned to the emission maxima. With decreasing cavity size, the spectra lose complexity, since less and less modes have sufficiently high Q-factors to overcome the increasing losses due to the increasing curvature of the surface. Moreover, the free spectral range, $\delta\lambda = \lambda^2/(2\pi n_{\mathrm{c}} R + \lambda)$, depends inversely on R, thereby further reducing the number of modes within the emission range of the dye.

In Fig. 2, the WGM with $q = 1$ have been assigned to their theoretical values by a least square fit of the resonance positions as pointed out in the experimental section. The eccentricity of the particles, i.e. the ratio $\mathrm{d}R/R$, was always below 5%, so that we may assume that the modes are degenerate in the quantum number m. Therefore, only the quantum numbers q and n will be considered in the following. Except for the spectrum of the 20 μm particle, where only the $q = 1, n = 180$ modes have been marked for the sake of clarity, all $q = 1$ modes have been assigned in the spectra. While the larger particles exhibit also modes with higher q, i.e. modes lacking any assignment, the smallest two particles show only $q = 1$ mode excitations. This observation exemplifies that losses in these particles have become significant and only those modes with the highest Q-factors survive, while all others are quenched. The $q = 1$ modes propagate most closely to the interface and thus, have the highest incidence angles, thereby facilitating fulfillment of the TIR condition. Accordingly, they are least affected by the increase in curvature with decreasing R and do still persist while higher q modes are already damped out. They also, however, suffer from the increasing losses as can be concluded from the significant line broadening. For comparison, the linewidths of different TE and TM modes and particle sizes are given in Table 1.

Particles with 1.5 μm diameter are the smallest for which we achieved excitation of WGM. The extreme broadening of the lines indicates a practical limit for WGM excitation. A reasonable trade-off between miniaturization and spectrum quality is found at 2 μm diameter. Therefore, we tested the 2 μm beads for their sensitivity towards biomolecular adsorption using BSA as a model protein. As displayed in Fig. 3, a clear shift of 0.86 nm is observable, which is in line with [12]

$$\frac{\Delta\lambda}{\lambda} = \frac{\alpha_{\mathrm{BSA}}\sigma_{\mathrm{s}}}{\varepsilon_0 \left(n_{\mathrm{c}}^2 - 1\right) R}, \tag{4}$$

which yields $\Delta\lambda = 0.73$ nm[1]. In (4), α_{BSA} is the polarizability of the BSA molecules and σ_{s} their surface density on the particle surface.

This promising finding highlights that the $1/R$ law is valid even down to few microns in cavity size with a corresponding sensitivity increase, although the total area of the particle

[1] Calculated for $R = 1$ μm. $\sigma_{\mathrm{s}} = 2.9 \times 10^{12}$ /cm^2 is the surface density of BSA molecules on the particle surface as determined by Arnold et al. [13], while we calculated the polarizability $\alpha_{\mathrm{BSA}} = 4\pi\varepsilon_0$ (5.25×10^{-21} cm^3) for BSA in air on basis of the Clausius–Mossotti relation and the result given by Arnold et al. for the excess polarizability of BSA in water $\alpha_{\mathrm{ex}} = 4\pi\varepsilon_0$ (3.85×10^{-21} cm^3).

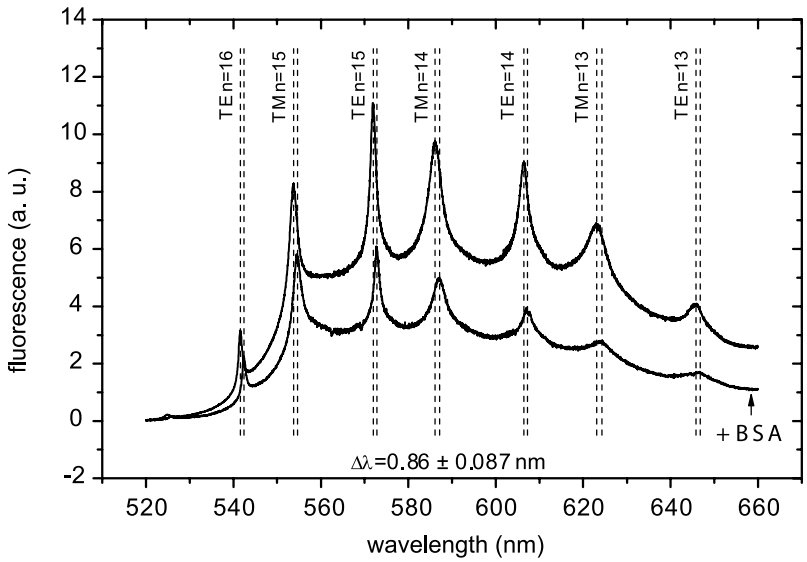

FIGURE 3 Emission spectra from a fluorescent 2 μm PS particle before and after adsorption of bovine serum albumin (BSA)

Size (μm)	Mode	Position (nm)	FWHM (nm)	Q-factor
20	TM $q=1, n=190$	568.8	0.63	897
	TE $q=1, n=190$	570.3	0.26	2180
	TM $q=1, n=180$	599.3	0.65	925
	TE $q=1, n=180$	601.0	0.33	1828
6	TM $q=1, n=45$	556.8	0.78	716
	TE $q=1, n=45$	563.8	0.77	732
	TM $q=1, n=44$	568.2	0.95	600
	TE $q=1, n=44$	575.7	0.68	845
2	TM $q=1, n=15$	552.8	2.43	227
	TE $q=1, n=15$	571.0	1.68	340
	TM $q=1, n=14$	585.0	3.76	156
	TE $q=1, n=14$	605.3	2.50	242
1.5	TM $q=1, n=11$	566.9	14.19	40
	TE $q=1, n=11$	590.0	9.48	62
	TM $q=1, n=10$	613.2	36.53	17
	TE $q=1, n=10$	643.0	12.19	53

TABLE 1 Positions, bandwidths (full width at half maximum), and Q-factors of selected TM and TE modes in dependence of the particle size. Corresponding WGM spectra are shown in Fig. 2

– and thus its load – decreases with $1/R^2$. Assuming a BSA density [12] of $\sigma_s = 2.9 \times 10^{12}$ molecules/cm^2, a molecular weight of 66 kDa, and a peak shift resolution of 0.1 nm, the detection limit of our system is 4.6 fg. To confirm this encouraging result, we selected a well-characterized system for precise determination of the peak shift in dependence of the adsorbate film thickness by successively depositing layers of oppositely charged PE onto the particles from 0.5 M NaCl aqueous solutions [21, 23]. The inset of Fig. 4 shows the peak shift as a function of the number of adsorbed PE layers for four different WGM. Within the experimental error, all four peaks exhibit the same shift. After three layers, a significant increase in the slope is observed.

To exclude that salt crystallites remaining in the PE film after drying induce this increase, we adsorbed PE also from salt-free solution. For direct comparison, Fig. 4 shows the average resonance shift[2] as a function of layer thickness for deposition from salt-free and 0.5 M NaCl solution, respectively. Thickness was calculated on the basis of a neutron reflectometry study [23][3], using for the thickness of a single PAH/PSS-bilayer 8 Å under salt-free conditions and 35.6 Å in 0.5 M NaCl solution, respectively, with a contribution of PSS to these values of 76%. Both experimental series (with and without salt) show the same behavior within the error including an increase in the slope for thicknesses beyond 40 Å. A linear fit of the data from 1 to ~ 40 Å yields a slope of 0.038 nm/Å. This value[4] is in good agreement with (4), which predicts 0.032 nm/Å. So it is interesting to see what happens beyond that point.

The perturbation theory used by Arnold et al. [13] for derivation of (4) neglects any increase in particle diameter due to adsorption, which, however, might contribute to the shift as $\frac{\Delta\lambda}{\lambda} = \frac{n_L}{n_c}\frac{d}{R}$, where d is the thickness of the adsorption layer and n_L its refractive index. To account for all potential effects in an accurate fashion, we performed spectrum simulations based on Mie theory for coated spheres as developed by Aden and Kerker [19]. In Fig. 4, the resulting peak shifts are indicated by the solid diamonds. A linear dependence on the layer thickness with a slope of 0.042 nm/Å is observable, which is larger than the prediction of Arnold et al. [13], thus indicating that the perturbation theoretical approach lacks the dependence on layer thickness. Our experimental result for thin layers up to 40 Å is just in-between the two theoretical predictions, while the shifts are obviously larger beyond the thin film regime.

[2] Average over all four modes (TM 15, TE 15 and TM 14, TE 14).

[3] We used the thickness of the fully hydrated films as given in [23], since only for this case data on the refractive index of the PE layer was available [21]. This does not affect the further analysis, because the system is only sensitive to changes in optical thickness of the adsorbate layer, i.e. the quantity "thickness" × "refractive index". Further details are given in the electronic supplementary material.

[4] Assuming $R = 1$ μm and replacing the polarizability α_{BSA} by that of the polyelectrolytes α_{PE}, as calculated from the Clausius–Mosotti relation and a refractive index of the PE layer of $n_{PE} = 1.47$. The surface density σ_s of the PE layer was calculated using the relation $\varrho_{PE} N_A / M_w = \sigma_s / d$, where ϱ_{PE} is the density of the PE layer (cf. [22]), M_w its molecular weight, d its thickness, and N_A the Avogadro number.

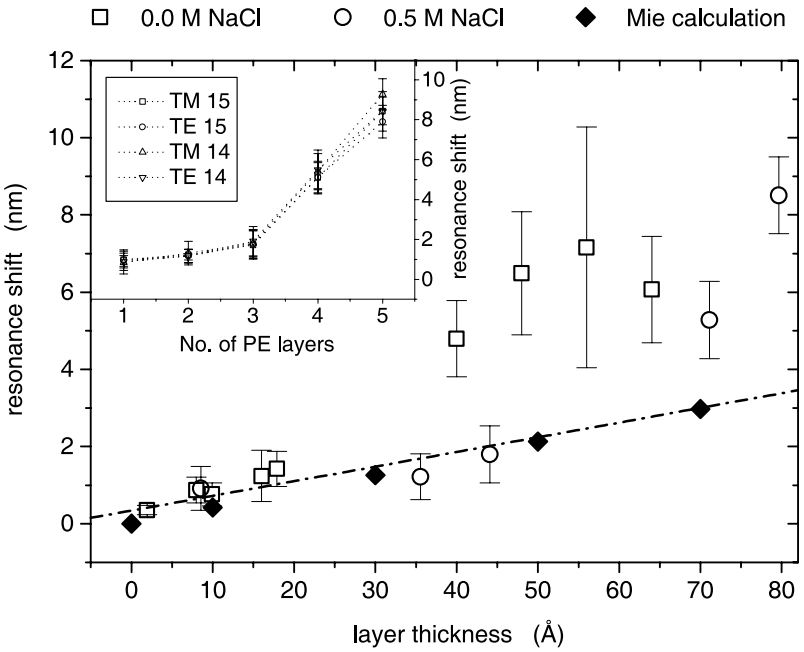

FIGURE 4 Calculated and measured shifts of the WGM resonance peaks of fluorescent 2 μm PS particles due to adsorption of polyelectrolyte (PE) multilayers. PE adsorption was performed from 0.5 M NaCl aqueous solution as well as from salt-free solution to exclude the impact of salt remaining in the adsorbed layer. The *inset* shows the measured shifts for four different modes in dependence of the number of adsorbed PE layers prepared from 0.5 M NaCl solution. The main graph displays the average over these four modes. The error bars indicate the standard deviation of the sample-to-sample variation. The *dash-dotted line* in the main graph corresponds to a linear fit of the measured peak shifts up to a PE layer thickness of 40 Å. The fit yields a sensitivity of 0.038 nm/Å in good agreement with the result of Mie theory, which yields 0.042 nm/Å (fit not shown). The measured sensitivity corresponds to a minimum detectable mass of PE of 3 fg, assuming a peak shift resolution of 0.1 nm

Assuming that Mie theory comprises a full description of the system, these deviations must be related to experimental uncertainties. Since we use surface-adsorbed particles, the contact area between particle and interface remains uncoated, which can explain the smaller experimental shift in the regime below 40 Å compared to Mie theory. Moreover, PE are known to form thicker adsorption layers after the first few double layers, an effect which has not been accounted for in the work of Lösche et al. [23], who calculated average layer thicknesses. Therefore, we possibly overestimate the thickness in the first regime, thus causing a reduction in slope, and underestimate it in the latter. In addition, side effects, such as the accumulation of material underneath the particles during the drying process [24], might come into play at higher layer thickness, since some material deposited on the substrate might be adsorbed only loosely, and thus be dislocated during the washing cycles. Systematic studies to reveal the observed deviation from Mie theory at high deposition thickness are currently under way.

4 Conclusions

We have demonstrated the feasibility of WGM sensing in the low Q-limit and shown that the predicted increase in sensitivity holds. The sensitivity of 0.038 nm/Å for the adsorption of PE layers translates into a detection limit of 3 fg, if we assume that a spectral shift in the WGM mode positions of 0.1 nm can still be detected. To understand how this sensitivity compares with other label-free methods for biosensing, we calculated the mass sensitivity (in pg/mm^2) and absolute detection limit (in pg) for a number of state-of-the-art methods based on their performance demonstrated in recent publications. The results are given in Table 2, and the details of the estimation in the electronic supplementary material.

Interestingly, the table exhibits the following rule of thumb: macroscopic methods, i.e. methods requiring a minimum surface area for detection of (100 μm)^2 and above, show very high mass sensitivity of a few pg/mm^2. However, they exhibit a rather high detection limit in terms of absolute mass, typically in the 100 pg regime due to the relatively large surface area used. In contrast, microscopic methods, such as micro-cantilevers or the low-Q WGM sensor presented in this article, have a lower mass sensitivity of some hundreds of pg/mm^2 due to higher fluctuations in microscopic systems, but reach very low detection limits of a few femtograms.

Method	Mass sensitivity (pg/mm^2)	Detection limit (pg)
surface acoustic waves	6–20	30–100
micro cantilever	460	5.5×10^{-3}
high-Q WGM	6	3
low-Q WGM	213	2.7×10^{-3}
surface plasmons	10	6.3×10^{-3} (4×10^{-5})
localized surface plasmons (large area)	47	253
localized surface plasmons (single Au particle)	(398)	(2×10^{-6})
composite systems (metal film + metal particle)	55	37×10^{-3}

TABLE 2 Mass sensitivities and detection limits for a selection of label-free optical methods for biosensing. Values in parentheses refer to theoretical extrapolations. The details of the derivation of these estimates are provided in the electronic supplementary material

This general trend might be broken by methods based on surface plasmon resonance (SPR), which are known to have a high mass sensitivity of 10 pg/mm^2, and potentially a lateral resolution limited only by the propagation length of the surface plasmons, i.e. 2–10 μm for thin gold or silver metal films. However, restricted by the low signal-to-noise ratio, state-of-the-art imaging SPR sensors reach a resolution of about (25 μm)^2, thereby limiting their potential for miniaturization [25].

Localized SPR of single metal nanoparticles promises an interesting alternative. Here, however, the amount of adsor-

bate on a single metal cluster is very difficult to determine and precise experimental values for mass sensitivity and detection limits have not been given in the literature so far. Therefore, only a theoretical limit based on a Mie simulation [26] is given in Table 2. Composite systems, which combine local and non-local SPR, seem to provide high mass sensitivity and low detection limit simultaneously as demonstrated in a number of studies [27–29]. The best lateral resolution practically reached in this case is $(25\,\mu m)^2$, and is therefore still significantly lower than that of the 2 μm particles used in the present study.

Altogether, we have shown that by means of WGM sensing in the low-Q limit a performance can be reached that is highly competitive with respect to other label-free methods for optical (bio-)sensing. The demonstrated detection limit of 3 fg and the overall size of 2 μm in diameter are currently unrivaled for label-free optical sensing, thus creating demand for practical applications of this miniature sensor in the future. Besides its sensitivity, one particular advantage of low-Q sensing is the small number of remaining WGM, which allows a dye-mediated excitation of the sensor. Accordingly, all mechanical constraints known from high Q-sensing are released and even remote sensing applications, such as microscopic in-vitro biosensing, seem to be in close reach.

ACKNOWLEDGEMENTS The authors are indebted to the Volkswagen-Stiftung for financial support in line with the funding initiative 'Complex Materials' (grant-no. I/79 466-7).

REFERENCES

1 K.J. Vahala, Nature **424**, 839 (2003)
2 A.B. Matsko, V.S. Ilchenko, IEEE Select. Top. Quantum Electron. **12**, 3 (2006)
3 V.S. Ilchenko, A.B. Matsko, IEEE Select. Top. Quantum Electron. **12**, 15 (2006)
4 J.M. Gérard, B. Sermage, B. Gayral, B. Legrand, E. Costard, V. Thierry-Mieg, Phys. Rev. Lett. **81**, 1110 (1998)
5 D.W. Vernooy, A. Furusawa, P. Georgiades, V.S. Ilchenko, H.J. Kimble, Phys. Rev. A **57**, R2293 (1998)
6 N. Le Thomas, U. Woggon, O. Schöps, M.V. Artemyev, M. Kazes, U. Banin, Nano Lett. **6**, 557 (2006)
7 J.L. Jewell, S.L. McCall, Y.H. Lee, A. Scherer, A.C. Gossard, J.H. English, Appl. Phys. Lett. **54**, 1400 (1989)
8 M. Kuwata-Gonokami, K. Takeda, H. Yasuda, K. Ema, Japan. J. Appl. Phys. **31**, L99 (1992)
9 L. Maleki, A.A. Savchenko, A.B. Matsko, V.S. Ilchenko, Proc. SPIE **5435**, 178 (2004)
10 S. Blair, Y. Chen, Appl. Opt. **40**, 570 (2001)
11 J.L. Nadeau, V.S. Ilchenko, D. Kossakovski, G.H. Bearman, L. Maleki, Proc. SPIE **4629**, 172 (2002)
12 F. Vollmer, D. Braun, A. Libchaber, M. Khoshsima, I. Teraoka, S. Arnold, Appl. Phys. Lett. **80**, 4057 (2002)
13 S. Arnold, M. Khoshsima, I. Teraoka, S. Holler, F. Vollmer, Opt. Lett. **28**, 272 (2003)
14 M.L. Gorodetsky, A.A. Savchenkov, V.S. Ilchenko, Opt. Lett. **21**, 453 (1996)
15 F. Vollmer, S. Arnold, D. Braun, I. Teraoka, A. Libchaber, Biophys. J. **85**, 1974 (2003)
16 T. Mukaiyama, K. Takeda, H. Miyazaki, Y. Jimba, M. Kuwata-Gonokami, Phys. Rev. Lett. **82**, 4623 (1999)
17 G. Schweiger, M. Horn, J. Opt. Soc. Am. B **23**, 212 (2006)
18 A.N. Oraevsky, Quantum Electron. **32**, 377 (2002)
19 A.L. Aden, M. Kerker, J. Appl. Phys. **22**, 1242 (1951)
20 A. Quirantes, A.V. Delgado, J. Phys. D **3**, 2123 (1997)
21 F. Caruso, H. Lichtenfeld, E. Donath, H. Möhwald, Macromolecules **32**, 2317 (1999)
22 G. Roll, T. Kaiser, G. Schweiger, Appl. Opt. **37**, 2483 (1998)
23 M. Lösche, J. Schmitt, G. Decher, W.G. Bouwman, K. Kjaer, Macromolecules **31**, 8893 (1998)
24 J. Boneberg, F. Burmeister, C. Schäfle, P. Leiderer, D. Reim, A. Fery, S. Herminghaus, Langmuir **13**, 7080 (1997)
25 J.M. Brockman, B.P. Nelson, R.M. Corn, Annu. Rev. Phys. Chem. **51**, 41 (2000)
26 G. Raschke, S. Kowarik, T. Franzl, C. Sönnichsen, T.A. Klar, J. Feldmann, A. Nichtl, K. Kürzinger, Nano Lett. **3**, 935 (2003)
27 M. Himmelhaus, H. Takei, Sens. Actuators B **63**, 24 (2000)
28 X. Hong, F.-J. Kao, Appl. Opt. **43**, 2868 (2004)
29 R. Dahint, E. Trileva, H. Acunman, U. Konrad, M. Zimmer, V. Stadler, M. Himmelhaus, Biosens. Bioelectron. **22**, 3174 (2007)